Acta Astronautica 215 (2024) 725–738

Contents lists available at ScienceDirect

Acta Astronautica

journal homepage: www.elsevier.com/locate/actaastro

Research paper

Joint determination of Venus gravity and atmospheric density through EnVision radio science investigation

Anna Maria Gargiulo [a,*], Antonio Genova [a], Flavio Petricca [a], Edoardo Del Vecchio [a], Simone Andolfo [a], Tommaso Torrini [a], Pascal Rosenblatt [b], Sébastien Lebonnois [c], Jean-Charles Marty [d], Caroline Dumoulin [b]

[a] Department of Mechanical and Aerospace Engineering, Sapienza University of Rome, 00184 Rome, Italy
[b] Nantes Université, Univ Angers, Le Mans Université, CNRS, Laboratoire de Planétologie et Géosciences, LPG UMR 6112, 44000 Nantes, France
[c] LMD/IPSL, Sorbonne Université, CNRS, Paris, France
[d] CNES/GRGS, Toulouse, France

ARTICLE INFO

Keywords:
Precise orbit determination
Gravity and radio science
Atmospheric drag
Deep space mission
Venus

ABSTRACT

The ESA mission EnVision will address its main scientific questions through a detailed mapping of the surface and interior properties of Venus. A precise reconstruction of the spacecraft trajectory is a key requirement for the EnVision scientific investigations, including radio science. To precisely constrain the orbit evolution, refined models of the dynamical forces are included in the Precise Orbit Determination (POD) process. We developed a methodology based on a batch-sequential filter that enables a joint estimation of Venus gravity and atmospheric density. Our approach yields an accurate compensation of atmospheric mismodeling, simulated through semi-empirical predictions of the atmospheric density provided by general circulation models (GCM), *e.g.*, Venus Climate Database (VCD). Numerical simulations of the EnVision radio science investigation were carried out by using a perturbative analysis of the dynamical forces, which accounts for atmospheric density errors ≥ 200%. By adjusting a set of atmospheric scale factors, our proposed strategy enables an estimation of the atmospheric density at the spacecraft altitudes with an accuracy of 25%. The improved dynamical model yields accuracies in the orbit reconstruction of 1–2 m, 30–40 m and 20–30 m in the radial, transverse and normal directions.

1. Introduction

A new phase of Venus' exploration is approaching with three space missions selected to unveil the secrets of the planet, the NASA Deep Atmosphere Venus Investigation of Noble gases, Chemistry and Imaging (DAVINCI) [1] and Venus Emissivity, Radio Science, InSAR, Topography, and Spectroscopy (VERITAS) [2] missions, and the ESA EnVision mission [3,4]. This unprecedented multidisciplinary dataset will enhance our knowledge of the mechanisms that led to the different evolution of Venus and Earth in spite of similar size, bulk composition and distance from the Sun [5]. Previous space missions, *e.g.*, Pioneer Venus Orbiter (PVO) and Magellan, revealed a relatively young surface [6–8] providing evidence of abundant volcanic and tectonic features, including *coronae* (*i.e.*, quasi-circular volcano-tectonic structures) and *tesserae* (*i.e.*, sets of curved, parallel linear features) [9], and randomly distributed craters. Whether Venus is still active today is an open question, recent support for this hypothesis was provided by the results of the re-analysis of Magellan Synthetic Aperture Radar (SAR) mapping [10] and by the surface thermal emissivity data collected by the Visible and Infrared Thermal Imaging Spectrometer (VIRTIS) onboard Venus Express [11]. Additional evidence is provided by the high content of sulphure dioxide [12] in the Venus' atmosphere and the surface's mineralogy and composition derived from visible to near-infrared (VNIR) reflectance spectra [13] observed by the Venus Express probe. EnVision will significantly contribute to better understand the level and nature of current geological activity through a SAR system that supports imaging with a spatial resolution an order of magnitude higher than Magellan, a Subsurface Radar Sounder (SRS) that provides direct measurements of subsurface features (*e.g.*, magma deposits), and an advanced instrument suite [3].

Furthermore, the determination of Venus' gravity field and tidal response is among the primary objectives of EnVision science investigation. To date, the most updated solution of Venus' gravity field is based on the radio science data collected by the PVO and Magellan missions [14,15]. However, these measurements were not sufficiently

* Corresponding author.
E-mail address: annamaria.gargiulo@uniroma1.it (A.M. Gargiulo).

https://doi.org/10.1016/j.actaastro.2023.12.010
Received 21 June 2023; Received in revised form 27 November 2023; Accepted 5 December 2023
Available online 13 December 2023

accurate to constrain Venus' internal structure, including the state of the planet's core, and the properties of the mantle. Based on the analysis carried out by Dumoulin et al. [16] and Margot et al. [17], the estimated value of Venus' moment of inertia (MOI) is in the range 0.327–0.342 and 0.313–0.361, respectively, providing rough constraints on the radius of the core in a range of 2900–3450 km and $\sim 3500 \pm 500$ km. Our current knowledge of the Love number k_2 ($\sigma_{k_2} = 0.066$ [15]) prevents a thorough characterization of Venus' core. The estimated gravity tidal response is consistent with a fully solid and a liquid/partially melted core [16,18]. An enhanced measurement of the Love number k_2 is then fundamental to improve our knowledge of the planet's deep interior. A first observation of the tidal phase would also inform on the composition, viscosity and rheology of the mantle. EnVision radio science investigation is expected to provide these measurements enabling key constraints on the properties of Venus' core and mantle [19,20].

To accomplish these scientific objectives, an accurate reconstruction of the spacecraft trajectory is a key requirement that can be fulfilled through a precise modeling of the dynamical forces included in the Precise Orbit Determination (POD) process. Spacecraft in orbit around Venus have to face the challenging conditions imposed by the harsh Venus' environment, with the atmospheric drag due to the planet's thick atmosphere being among the main non-conservative forces. Therefore, accurate predictions of Venus' atmospheric density will be essential to evaluate the atmospheric drag acceleration acting on the EnVision spacecraft and improve its orbit determination.

General circulation models (GCM) have been developed to model Venus' atmosphere and provide predictions of the properties and dynamics of its lower layers (*i.e.*, 48–70 km altitudes) that are dense, hot and characterized by thick clouds. These models account for the fast rotational state of the atmosphere with zonal winds up to 100 m s^{-1} near the cloud top (*i.e.*, super-rotation) and the vortex structures centered around the poles at latitudes $\geq 60°$.

The Venus Global Reference Atmospheric Model (Venus-GRAM) [21] and the Venus Climate Database (VCD) [22] are two well consolidated models that predict the properties of Venus' atmosphere. These two models, however, are based on different methods and assumptions, including topography, accuracy of the model of diurnal cycle, variation of Venus density with solar activity, dependence on cloud albedo variability, and on the analysis of different data collected by previous missions. These discrepancies are mainly associated with unpredicted mismodeling of Venus' atmospheric parameters due to the lack of accurate measurements and limitations in the theoretical models. These uncertainties may affect the trajectory reconstruction of Venus' orbiters, leading to undesired errors in the estimation of the planet's gravity field and geophysical parameters (*e.g.*, Love number k_2) through radio science investigation.

In this paper, we present a method that enables the precise orbit determination (POD) of the ESA EnVision mission and the joint determination of Venus' gravity and atmospheric density. The EnVision spacecraft will be inserted in a 220 × 520 km quasi-polar (with inclination between 87° and 89°) orbit about Venus during its science phase. A mismodeling of the atmospheric drag acceleration at the periapsis may have a significant impact on the orbit reconstruction, and, consequently on the determination of Venus' gravity field. The altitude region above ~180 km and the thermosphere above 250 km represent regions of Venus' atmosphere that have not been extensively probed by dedicated instruments, resulting in limited information on the atmospheric density and other thermodynamical properties [23]. Venus' atmospheric models yield density profiles at those altitudes through upward integration of the properties related to the lower atmospheric layers where temperature profiles and species concentration were obtained through *in situ* campaigns. Measurements acquired through infrared spectrometry from Venera-15 orbiter and Venus Express observations in the ultraviolet (UV) and infrared (IR) range probed the middle atmosphere of Venus and enabled the characterization of CO_2, SO_2, SO clouds and aerosol temperature vertical evolution in the range of 60–160 km altitudes [24,25]. Complementary information was provided by radio occultation experiments, *e.g*, the density profiles from 40 to 90 km obtained by Venus Express Radio Science experiment (VeRa) [26] or inferred from spacecraft's orbital decay [27–29]. Further constraints will be determined by EnVision's radio occultations and direct measurements of EnVision's spectrometers suite VenSpec.

A comparison of the predicted atmospheric densities at the spacecraft orbital altitudes based on the Venus-GRAM and VCD atmospheric models indicates strong differences that need to be accounted for in a realistic assessment of the EnVision orbit reconstruction requirements. Similar discrepancies may be expected between the real values and the predictions from the models. We thus carried out a perturbative analysis by assuming a different modeling of the atmospheric drag forces between the simulation of the synthetic data and the POD process. An estimation method that was named *batch-sequential* and conceived by Genova et al. [30] for the data analysis with uncertain dynamical models is then used to process the EnVision radio science data and to compensate atmospheric mismodeling.

This paper is organized as follows. In Section 2, we introduce the EnVision mission configuration and radio tracking system (Section 2.1), and the theoretical background of the work, including the implementation of the classical batch filtering and the batch-sequential filtering (Sections 2.2.1 and 2.2.2). In Section 3, we present the force models implemented in our POD process, with a focus on the atmospheric drag. Two Venus' atmospheric models are described, *i.e.*, the Venus-GRAM and the VCD (Section 3.2.1), and a preliminary analysis of the discrepancies in terms of induced impulsive $\Delta V s$ during the spacecraft orbit associated with the two different atmospheric models is reported in Section 3.2.2. The results of our numerical simulations of the EnVision radio science investigation are shown in Section 4. The steps that we adopted to carry out the perturbative analysis are described in Section 4.1, and the estimation strategies are discussed in Section 4.2. Finally, the discussion and summary of the results are provided in Sections 5 and 6, respectively.

2. Data and methods

2.1. EnVision radio tracking system

The entire science phase of the EnVision mission is expected to cover 6 Venus' sidereal days (*i.e.*, six cycles, 243 Earth days each). In this study we considered the orbital configuration *EnVision_ESC_T4_2032_North VOI_v02* that foresees Venus Orbit Insertion over the northern hemisphere accordingly to the EnVision SPICE kernels [31]. The nominal mission baseline is scheduled from 15 June 2035 to 14 June 2039.

The spacecraft is equipped with a fixed High Gain Antenna (HGA) to establish X-band uplink and a dual X-Ka band frequency downlink with the ground stations of the ESA ESTRACK network. Doppler data are acquired during daily scheduled tracking passages of ~3.5 h. To explain the benefits of the dual-link configuration, we describe below the noise sources of the radio tracking data.

The total noise budget of the Doppler data is obtained by including thermal, tropospheric and solar plasma contributions (Fig. 1 based on [32]). EnVision communication to ground will be established through the HGA enabling a high signal-to-noise ratio that will limit the effects of the thermal noise. Troposphere and interplanetary plasma are then the dominant noise sources. The propagation delay in the troposphere is mainly affected by the seasonal variability at the ground station site. The wet component of the troposphere also affects the Doppler measurements depending on the weather conditions. To account for this unpredicted variation of the wet troposphere, we use a conservative value for the Doppler noise in our numerical simulations. GNSS-based calibration techniques at the ESTRACK ground stations are

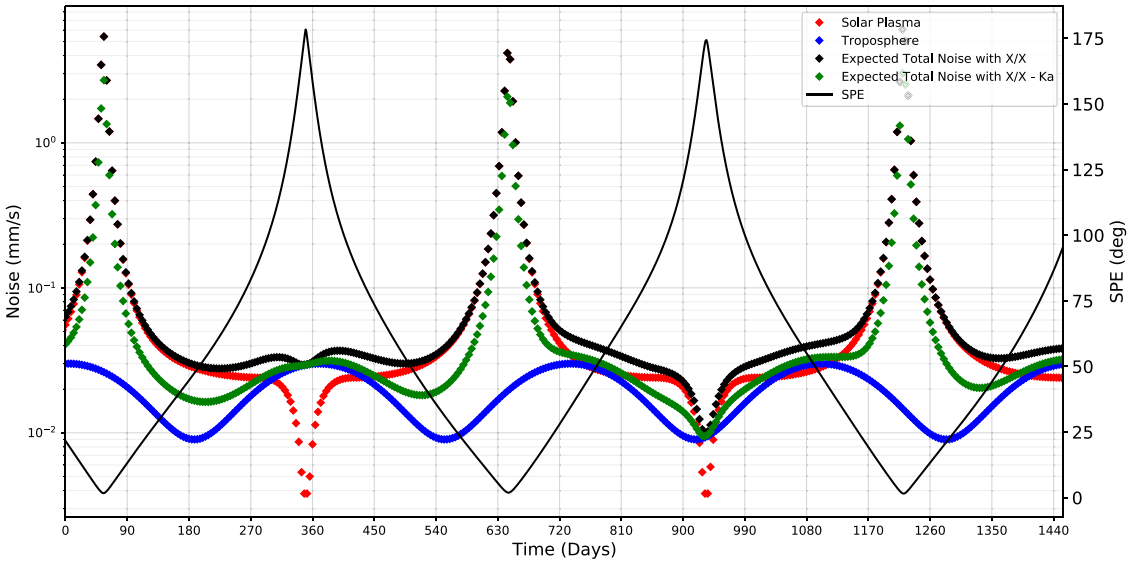

Fig. 1. Noise budget of the two-way Doppler measurements with X-band only (black) and X/X-Ka dual link configuration (green). The solar plasma contribution (red) varies with the SPE angle (black curve). The contribution due to the troposphere (blue) shows a periodic pattern associated with seasonal variations at the ground station site. We present this noise source associated with a ground station in the Earth's northern hemisphere (day 0 corresponds to 15 June 2035). (For interpretation of the references to color in this figure legend, the reader is referred to the web version of this article.)

expected to partially correct the tropospheric effects. The blue curve in Fig. 1 is obtained for a ground station in the northern hemisphere.

The primary source of noise that affects X-band Doppler measurements is the fluctuations in the electron content of interplanetary plasma. Solar plasma effects depend on the Sun-probe and probe-Earth (SPE) relative positions. This noise source has a significant impact on the total budget in proximity of superior solar conjunctions (*i.e.*, SPE $< 15°$). During EnVision science phase that will last six Venus' cycles, three solar conjunctions will strongly affect the noise budget of the radio science data. Doppler data acquired with a SPE angle less than 15° are then excluded from the POD process. The coherent dual frequency transmission (X-Ka band) for the downlink carrier enables a partial calibration of the plasma perturbation [33] for the remaining science phase (*i.e.*, SPE $> 15°$).

The fractional frequency shift y (*i.e.*, Doppler measurement normalized by the reference frequency) can be expressed as the sum of: (**1**) a non-dispersive term (y_{nd}) affected by the projection of the velocities difference along the line-of-sight and by the tropospheric noise; and (**2**) a dispersive term that differs between uplink (y_{up}) and downlink (y_{dn}) depending on the frequency of the signal and on the fluctuations of the Total Electron Content (TEC) along the path (*i.e.*, the total number of electrons between the radio transmitter and receiver). For a two-way Doppler measurement the fractional frequency shift is then given by:

$$y = y_{nd} + \frac{P_{up}}{f_{up}^2} + \frac{P_{dn}}{f_{dn}^2}, \tag{1}$$

where P_{up} and P_{dn} represent the TEC, and f_{up} and f_{dn} are the uplink and downlink carrier frequencies, respectively. By solving Eq. (1) for the dispersive term in downlink y_{dn}, the calibrated fractional frequency shift y^* can be evaluated as follows,

$$\begin{cases} y_{xx} = y_{nd} + \frac{P_{up}}{f_{up,x}^2} + \frac{P_{dn}}{f_{dn,x}^2} = y_{nd} + y_{up} + \frac{y_{dn}}{\alpha_{xx}^2} \\ y_{xk} = y_{nd} + \frac{P_{up}}{f_{up,x}^2} + \frac{P_{dn}}{f_{dn,k}^2} = y_{nd} + y_{up} + \frac{y_{dn}}{\alpha_{xk}^2}, \end{cases} \tag{2}$$

$$y_{xx}^* = y_{xk}^* = y_{nd} + y_{up} = \frac{\alpha_{xx}^2 y_{xx} - \alpha_{xk}^2 y_{xk}}{\alpha_{xx}^2 - \alpha_{xk}^2} \tag{3}$$

where $\alpha = \frac{f_{dn}}{f_{up}}$ is the turn-around ratio and $y_{dn} = \frac{P_{dn}}{f_{up,x}^2}$.

As shown in Fig. 1, the dual-link configuration (green curve) leads to enhancements of up to 50% with respect to a X-band radio system when the interplanetary plasma noise is dominant. However, in our analysis we consider a conservative level of noise (black curve) that accounts for uncalibrated troposphere and solar plasma with an average noise root-mean-square (RMS) of ~0.07 mm/s at 10 s integration time (that corresponds roughly to ~0.028 mm/s at 60 s integration time). This assumption is consistent with a single X/X link configuration. Gravity investigations will benefit from the partial plasma calibration to improve the estimates of Venus' gravity field and geophysical parameters, however, for the purpose of this paper, which is the assessment of the atmospheric drag effect on the orbit evolution, we preferred to use a conservative level of noise.

2.2. Precise orbit determination

2.2.1. Least-squares filter

Techniques for orbit determination problems are commonly based on least-squares filtering that is used to estimate a set of parameters that leads to a minimization of a cost function that depends on the observation residuals (*i.e.*, difference between the computed and observed measurements) [34]. This method applied to real data analysis is affected by instability issues that may be caused by mismodeling in the dynamical equations (*e.g.*, unpredicted variations of the non-conservative forces). Inconsistent predictions of the forces that act on the spacecraft motion lead to error accumulation on the reconstructed trajectory. Therefore, to prevent inaccurate least-squares solution, the total time span of the mission is divided in intervals (arcs) and additional adjusted parameters are introduced (*e.g.*, stochastic accelerations). This strategy then entails an over-parameterization of the problem through the adjustment of quantities that vary arc by arc (*e.g.*, spacecraft state vectors, ΔV maneuvers, set of accelerations), and, for this reason, are named local. The estimation of these additional parameters mitigates the errors caused by unmodeled dynamical effects, leading to significant enhancement in the retrieval of time-independent parameters, named global, that affect all the measurements.

After a single-arc processing of each arc that enables the adjustment of local parameters only, the final solution is recovered with a global inversion that accounts for both local and global parameters.

2.2.2. Batch-sequential filter

Following the approach proposed by Genova et al. [30], we developed a batch-sequential filter that copes with the mismodeling that affects the predictions of the properties of Venus' atmosphere. Possible errors in the drag modeling require the adjustment of a significant number of local parameters in the least-squares method. Different techniques have been used for Venus and Mars missions, including the estimation of a drag coefficient per orbit or periodical accelerations [29, 35].

We present an implementation of the batch-sequential filter (shown in Fig. 2) based on the definition of a set of global parameters that are adjusted in the intermediate batch inversion. These parameters are scale factors that are applied to the atmospheric density predictions based on Venus' atmospheric model (*i.e.*, Venus GRAM 2005) embedded in the POD software. Each coefficient is associated with a specific altitude range of the atmosphere. The atmospheric model is thus refined as new data are included in the estimate through the adjustment of the global atmospheric parameters (see Section 4.2). A sequential update of these scale factors is included to refine the dynamical model in the intermediate batches of data. The convergence of the solution is very sensitive to the choice of the number of estimated global parameters and to the number of arcs included in a single batch. A dedicated testing and validation test campaign was carried out to establish the properties of the batch-sequential filter. We note that the adjustment of a significant number of atmospheric scale factors associated with different altitude regions prevents the convergence of the solution since the radio tracking data are poorly sensitive to those parameters. On the other hand, the adjustment of a single scale factor is not well-suited to fully compensate Venus' atmosphere mismodeling. We then account for 3 parameters that scale the atmospheric density predictions at altitude ranges of 220–320 km, 320–420 km and 420–520 km, respectively. A similar trade-off results from a test campaign devoted to determine the number of arcs included in each batch. We use 20 arcs to account for the seasonal variability of Venus' atmosphere.

As shown in Fig. 2, the entire dataset of observed Doppler measurements is divided in N arcs, which are organized in N_B batches. Each batch j, with $j = 1, \dots, N_B$, is composed of n arcs ($N_B = N/n$) and it is processed accordingly to the following steps. First, a single arc estimation of the n arcs of the first batch is carried out and local parameters only are adjusted with an iterative process until convergence of the solution. A combined analysis of the data of the first batch is then carried out to jointly estimate the local parameters and the atmospheric scale factors. The initialization of the first batch consists in assuming as *a priori* uncertainties and values of the local parameters their *a priori* uncertainties and estimates from the single-arc estimation, respectively. Since the atmospheric scale factors are adjusted for the first time in this batch, no *a priori* uncertainty is assumed enabling an unconstrained solution. The global inversion of the intermediate batch is iterated until convergence. The scale factors adjustment retrieved after the batch inversion is then used to update the atmospheric modeling for the processing of the following arcs that are included in the next intermediate batch. From the second batch, the *a priori* uncertainties of the atmospheric parameters are obtained by multiplying their formal uncertainty resulting from the previous batch by a scale factor equal to 10. To prevent the filter from losing sensitivity to the new measurements, we re-initialize the filter after a certain number of batches. This process consists in setting the nominal values of the atmospheric scale factors equal to the estimated values retrieved from the previous batch, while their *a priori* uncertainties are re-initialized, meaning that they are set equal to a very high value, *i.e.*, 10. In our numerical simulations we enforce the filter re-initialization after 5 batches. This allows us to sequentially update atmospheric densities by using about two entire Venusian cycles.

After convergence of the last batch, we carry out an iterated single-arc estimation that assumes as *a priori* values the updated local parameters resulting from each batch and the final adjustment of the Venus' atmospheric profile from the last batch. This further process enhances the consistency amongst the trajectory of all the arcs that are now integrated with the same dynamical model (*i.e.*, no adjustment of the global parameters). By analyzing the measurement residuals, we are able to assess the accuracy of the POD solution.

A final step is a combined analysis of the radio tracking data of the entire dataset through a joint adjustment of the local parameters and the global atmospheric scale factors, whose nominal values result from the batch-sequential processing, and Venus' gravity and tides. This final global inversion allows us to determine the converged spacecraft trajectories, gravity field and atmospheric model parameters.

The proposed method represents an enhancement with respect to the alternative techniques since the sequential update of the dynamical model through the analysis of intermediate batches of data enhances the accuracy and the stability of the solution. A single global inversion after the single-arc processing of the entire datasets requires the adjustment of additional parameters, as, for example, stochastic accelerations, leading to higher formal uncertainties of the parameters of interest (*e.g.*, gravity field coefficients). Testing and validation of this batch-sequential filter are carried out with EnVision numerical simulations as reported in Section 4.

3. Dynamical force models

The trajectory integration of a spacecraft in orbit about Venus requires an accurate modeling of the dynamical forces and the physical properties of both the central body and the probe (*e.g.*, shape, thermo-optical coefficients, gravity field). Our numerical simulations are carried out through the JPL software MONTE Project Edition [36]. The main dynamical models in the POD software are the gravitational field of Venus and the non-conservative forces acting on the spacecraft, including the atmospheric drag, the solar radiation pressure, the albedo and the wheel off-loading maneuvers. A precise modeling of the spacecraft's shape is also fundamental for the computation of those perturbations. In our numerical simulations, we account for a simplified spacecraft model that is a cannon-ball shape based on EnVision's cross-section, with a ballistic coefficient close to 25 kg/m^2 [4]. In this section, we describe the main force models that significantly impact the spacecraft orbit evolution.

3.1. Gravitational field

The gravitational field of Venus is modeled through a spherical harmonic expansion [37],

$$U = \frac{GM}{r}\left\{1 + \sum_{l=2}^{m}\left(\frac{a_e}{r}\right)^l \sum_{m=0}^{l}\left[\bar{C}_{lm}\cos m\lambda + \bar{S}_{lm}\sin m\lambda\right]\bar{P}_{lm}(\sin\phi)\right\}, \tag{4}$$

where $GM = 324858.59$ km^3/s^2 is Venus gravitational parameter, $a_e = 6051.0$ km is Venus' reference radius [14], $\bar{P}_{lm}$ are the normalized associated Legendre polynomials of degree l and order m, and $\bar{C}_{lm}$ and $\bar{S}_{lm}$ are the normalized spherical harmonic coefficients [38]. The spherical harmonic expansion is expressed in the Venus' body-fixed frame that accounts for the planet's rotational parameters [39], with the spherical coordinates r, λ and ϕ that are radial distance, longitude and latitude, respectively.

The *a priori* gravity field used in our simulations is the MGNP180U model expanded to degree and order 180 [14]. This field is based on the gravity solution derived from the radio tracking data of NASA PVO and Magellan [14,15]. We also include the effect of the tides exerted by the Sun on the planet by assuming $k_{20} = k_{21} = k_{22} = 0.295$ for the real part and zero for the imaginary part [15]. Our simulations are based on the JPL planetary ephemerides DE432s [40].

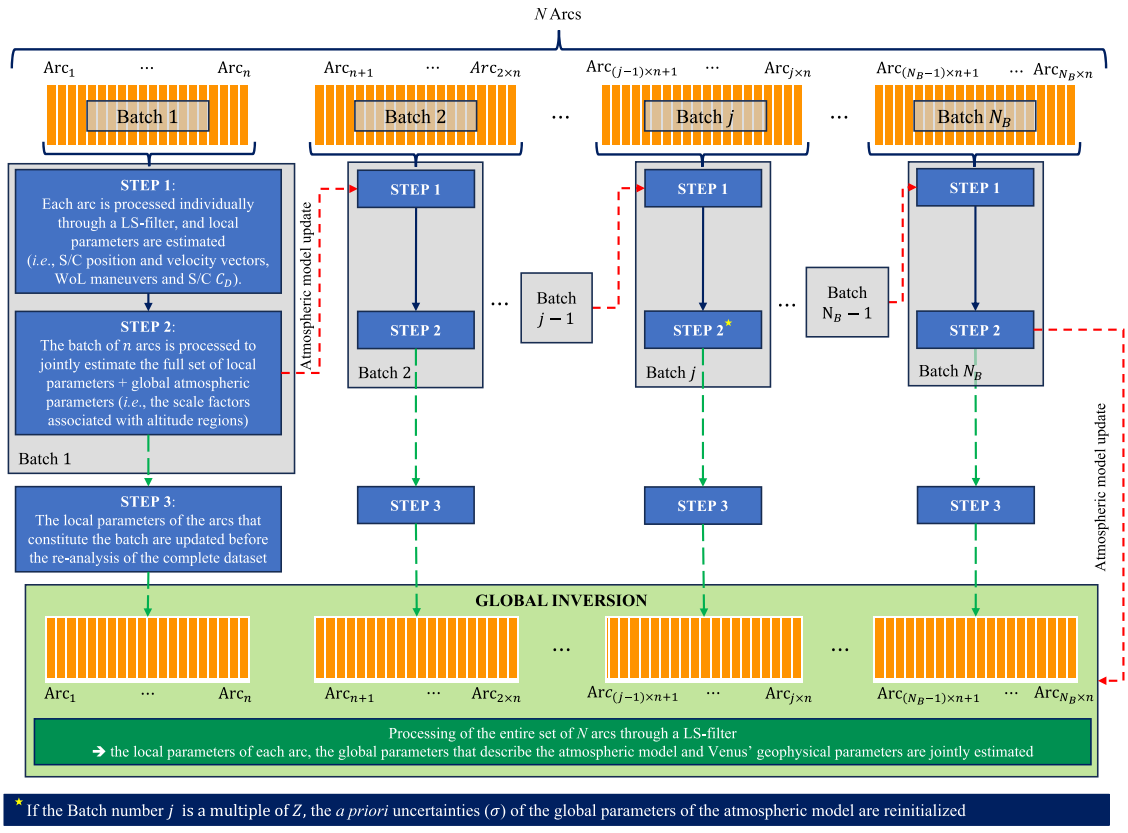

Fig. 2. Block diagram of the batch-sequential filter adopted for the POD of the EnVision mission. The set of N arcs is divided into N_B batches of n arcs, which are processed following the steps 1–3 summarized in the diagram. The estimates of each batch are used to sequentially update the atmospheric model used as *a priori* in the next batch. A re-initialization of the *a priori* uncertainties associated with the atmospheric scale factors is performed after a number Z of batches is analyzed (Z is among the parameters of the method that have to be set through test campaigns). The last batch provides the *a priori* atmospheric model that is implemented in the global inversion. The local parameters estimated at the end of each batch are used to initialize the spacecraft's state, WoL and C_D coefficients of the global inversion.

3.2. Non-conservative forces

An accurate modeling of the non-conservative forces is crucial to fulfill orbit reconstruction requirements. An important contribution is provided by the radiation pressure associated with the solar irradiance and Venus' albedo and thermal emission. Our models include a solar irradiance that varies with the spacecraft relative distance to the Sun, and constant and uniform albedo and infrared thermal emissivity for Venus [41,42].

Because of EnVision mission configuration, an additional perturbation is related to the wheel-off-loading (WoL) maneuvers that are required for the desaturation of the reaction wheels. A preliminary scheduling of the maneuvers assumes one per day events ~1 h before a tracking window. Because of misalignment of the thrusters, each fire leads to uncompensated residual velocities. Impulsive burns are then included at the epoch of the planned maneuver constraining the components of the residual velocity ΔV in the along-track, cross-track and radial directions to a maximum value of 1 mm/s, which is based on the system expectations.

The atmospheric drag significantly affects the evolution of the spacecraft's orbit. Its contribution is strongly dependent on the atmospheric conditions, the spacecraft's orbital configuration and shape. The atmospheric drag acceleration is

$$a_{drag} = -\frac{1}{2}\frac{\rho C_D A V^2}{m}\hat{n_V}, \tag{5}$$

where ρ is the atmospheric density, C_D is the drag coefficient, m is the spacecraft mass, A is the spacecraft's effective area and V and $\hat{n_V}$ are the spacecraft velocity module and direction. This simplified expression is based on the cannon-ball shape assumption, while in a general case, the contribution due to any panel of the spacecraft's shape should be included in the computation of the atmospheric drag acceleration. This formulation is suitable to model the along-track effects, while it does not account for the lateral wind and aerodynamic lift. Errors in the atmospheric drag modeling have a strong impact on the orbit reconstruction, and, consequently, on the estimation of the geophysical parameters based on the analysis of the radio science data.

A first source of model uncertainty is related to the assumed value of the spacecraft's C_D [43], which depends on the shape and the flow regime. Possible values of the drag coefficient C_D range from 1.7 to 2.3 for existing spacecraft. The main issue for the drag accelerations is associated with the predictions of the atmospheric densities that strictly depend on local time and solar activity variabilities [44]. Atmospheric models are strongly affected by the lack of *in-situ* and remote sensing data preventing a highly accurate modeling of short- and long-term temporal and spatial variations. For our numerical simulations, we compared the two main models that are publicly available for Venus' atmosphere, *i.e.*, the Venus-GRAM [21] and the VCD [22]. The discrepancies between these two models may be indicative of the level of accuracies expected for the current knowledge of the atmospheric properties at the altitude of spacecraft orbits. In Section 3.2.1, we briefly discuss the main differences between Venus-GRAM and VCD at the altitude range of interest, and we then present the induced impulsive ΔVs discrepancies associated with the two models (Section 3.2.2).

3.2.1. Atmospheric modeling

The Venus-GRAM is an engineering oriented model of Venus' atmosphere developed at the Marshall Space Flight Center's (MSFC) Natural Environment Branch for the planet Venus [45]. The lower atmosphere model included in Venus-GRAM (heights ≤ 250 km) is based on the

Committee on Space Research (COSPAR) Venus International Reference Atmosphere (VIRA) [21]. The VIRA model was built by using Venera entry probes data and Pioneer Venus orbiter and probe data, but it lacks a solid planet model and a high resolution gravity field. The model is divided into three altitude regions: (**1**) the low atmosphere VIRA data, extending from 0 km to 100 km, which depends on height and latitude; (**2**) the middle atmosphere VIRA data (height between 100 km and 150 km), which has dependence on height and local solar time; (**3**) the high atmosphere VIRA data (height ranging from 150 km and 250 km) that depends on height and solar zenith data.

At heights ≥ 250 km and ≤ 1000 km the Venus-GRAM is based on a thermosphere model developed at the MSFC [45]. This model assumes as lower boundary conditions VIRA conditions and constituents at 250 km and uses constant temperature values above 250 km set equal to the local VIRA temperature at 250 km. The model assumes that particles are in diffusive equilibrium and the total pressure and the mass density are evaluated from constituent partial pressures and constituent number densities, respectively.

Venus-GRAM is designed to guarantee smooth transitions of the atmospheric variables by taking into account seasonal, geographic, and altitude variations, and it is, therefore, considered to be suitable for engineering applications at all altitude regions of the Venus' atmosphere. The model requires time, longitude, latitude and height in input and estimates mean values and statistical variations of the atmospheric properties, *i.e.*, pressure, density, temperature and number densities for CO_2, N_2, O, CO, He, N and H, zonal and meridional winds.

The model lacks a high resolution topography model of the planet, accounting for Venus reference ellipsoid. Furthermore, it does not incorporate the dependence of atmospheric parameters on solar activity, thus, variations that should affect altitudes ≥ 100 km are not included. Changes in heating rate due to cloud albedo variability are not modeled. The POD software MONTE includes the Venus-GRAM to retrieve prediction of the atmospheric densities for the computation of the drag.

The VCD model is a database of meteorological fields derived from Venus General Circulation Model (VGCM) numerical simulations of Venus' atmosphere, aimed at supporting engineering applications and scientific studies requiring accurate knowledge of the state of the Venusian atmosphere. The VGCM is developed at the LMD (Paris, France) laboratories of the Institute Pierre Simon Laplace (IPSL) [22, 46] and has been validated by analyzing the Pioneer-Venus, Magellan and Venus Express data. This model computes the 3D atmospheric circulation and climate accounting for radiative transfer through the gaseous atmosphere, non-local thermodynamical equilibrium (NLTE) processes, EUV heating, conduction and molecular diffusion in the thermosphere. Furthermore, the model simulates sub-grid processes (*e.g.*, convection in the boundary layer, non-orographic and orographic gravity waves) and implements photochemistry to control the atmospheric composition.

The VCD includes ground-to-thermosphere atmospheric variables and high resolution topography (23 pixel/deg), alternatively it uses a lower resolution grid (96 × 96 in longitude × latitude). Variability in the radiative output of the Sun, which occurs with different timescales due to solar flares, solar rotation and magnetic cycle of the Sun, is significant in the UV region of the solar spectrum that is the main responsible for the heating of Venus upper atmosphere (above 100 km). At the same time, the solar heating rate is directly dependent on the cloud albedo by means of a radiative transfer model. The VCD allows to account for various conditions of EUV input and cloud albedo. Three fixed levels of EUV flux can be selected, *i.e.*, standard, maximum and minimum, corresponding to a value of E10.7 factor of 140, 300 and 70 solar flux unit (1 sfu = 10^{-22} Wm^{-2} Hz^{-1}) at 1AU. Alternatively, customized level of EUV input or realistic EUV deduced from Earth date, taken from available E10.7 measurements, can be selected.

Three cloud albedo scenarios are also available. The standard cloud albedo is computed by using standard heating profiles based on [47] and it is provided with three EUV conditions, *e.g.*, standard, minimum and maximum. The low cloud albedo scenario is calculated using the maximum heating rate profile presented in [48] with a maximum ratio of 50%, for the standard EUV conditions. The high cloud albedo scenario is evaluated by decreasing the standard rate profile by 30% based on the standard EUV conditions.

Venus-GRAM and VCD were then derived from different observations and assumptions, leading to significant discrepancies in the predicted evolution of the atmospheric properties at the spacecraft altitudes. By focusing on the atmospheric density, which is the most relevant parameter to drag force modeling, Fig. 3 compares the values predicted by the two models for the same Venusian hour at several altitudes. The five heights approximately correspond to the periapsis of Magellan (Cycle 1–4 and Cycle 5), Venus Express, Akatsuki (the Venus Climate Orbiter), and EnVision, where the effect of the atmospheric drag perturbation mostly affects the orbital dynamics. The relative differences between the two models were computed by selecting the standard EUV condition and standard cloud albedo scenario as VCD input, and represent an intermediate case; higher discrepancies are observed in the case of standard cloud albedo and minimum EUV conditions, while high cloud albedo and standard EUV conditions and standard cloud albedo and maximum EUV conditions represent the most optimistic scenarios (we provide comparisons of the two models according to the various scenarios in the Supplementary Material S1–S4). As shown in Fig. 3, the VCD yields significantly higher densities compared to the Venus-GRAM at around noon Local True Solar Time (LTST) for altitudes lower than 200 km. At the same LTST but higher altitudes, the Venus-GRAM suggests larger values than the VCD. Strong discrepancies between Venus-GRAM and VCD are also observed at the poles for altitudes ≥ 180 km. Different predictions of the latitude and LTST variations from the two models are observed at high altitudes. The Venus-GRAM, for example, predicts a significant increase in the atmospheric density at night LTST for altitudes larger than 250 km. These inconsistencies thus pose fundamental questions on the reliability of atmospheric models for precise orbit determination and navigation tasks.

3.2.2. Impact of Venus atmospheric drag mismodeling on spacecraft orbit evolution

To better understand the impact of atmospheric mismodeling on the orbit evolution, we carried out dedicated numerical simulations to determine the energy dissipated along the spacecraft orbit by using the two independent models of Venus' atmosphere, Venus-GRAM and VCD. By integrating the drag acceleration with respect to time along the arc of the spacecraft trajectory affected by the atmosphere, we can determine the equivalent ΔV that results from the atmospheric density predictions. Given the spacecraft trajectory extracted from the SPICE kernels, the spacecraft's orbit was discretized into n_S segments that cover an altitude range Δh of 10 km in the altitude band 0–520 km. The resulting ΔV (associated with a single orbit) was computed according to:

$$\Delta V = \sum_{i=1}^{n_s} \frac{1}{2} \frac{\bar{\rho}_i C_D \bar{V}_i^2}{m} A \Delta t_i, \tag{6}$$

where m, C_D and A represent the spacecraft's mass, drag coefficient and effective area, respectively. The ballistic coefficient is assumed to be 25 kg/m^2. The mean density $\bar{\rho}_i$ and velocity $\bar{V}_i$ are computed for each ith segment of the orbit and Δt_i is the duration of the segment. We applied this methodology to compute the induced ΔVs for each orbit for an entire Venusian day by assuming EnVision, Magellan (Cycle 5), and Venus Express missions. We include in our analysis the aerobraking phase of Venus Express that took place in June–July 2014 to gradually reduce the pericenter altitude from 200 km to 130 km. We show the discrepancies between the ΔVs computed by using the Venus-GRAM and VCD for the three orbiters in Fig. 4 (panels A, B and C). The

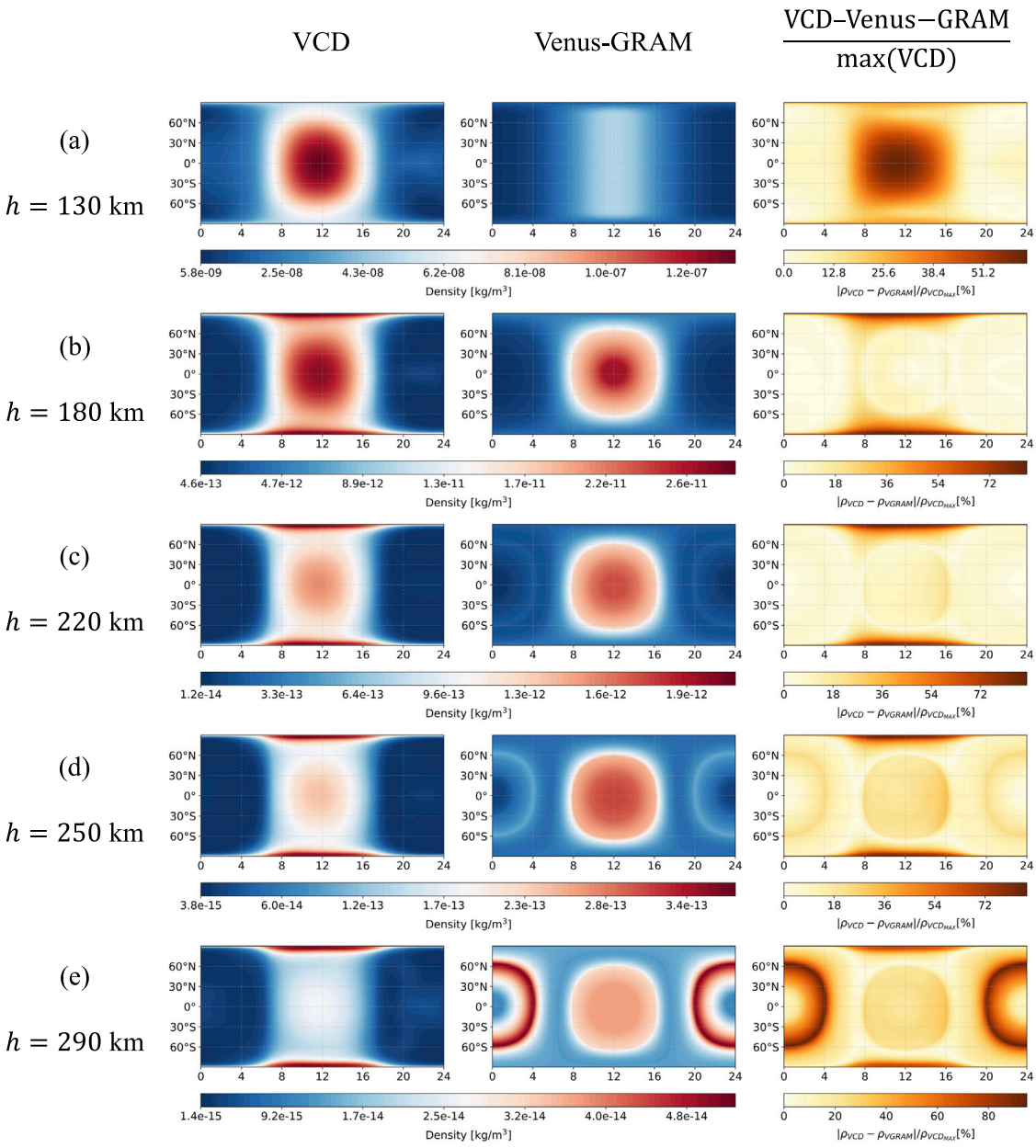

Fig. 3. Latitudinal and LTST maps of the discrepancies between the density profiles predicted by the VCD (**left**) and the Venus-GRAM (**central**) computed at different altitudes above Venus' reference sphere (radius 6051.8 km). Rows (a–e) show the results obtained at 130 km, 180 km, 220 km, 250 km, and 290 km, which represent approximately the minimum altitude reached by Venus Express, Magellan (Cycle 5), EnVision, Akatsuki, and Magellan (Cycle 1–4), respectively. The VCD predictions are based on the standard EUV and cloud albedo scenario. The right panels show the percentage error computed as the absolute value of the difference between the two models normalized by the maximum density predicted by the VCD.

histograms report the frequency of the $|\Delta V_{VGRAM} - \Delta V_{VCD}|$ values evaluated for each orbit during an entire Venusian day. The discrepancies between the two models lead to differences in the equivalent ΔV per orbit highlighting its dependency on the spacecraft orbit altitude. For Magellan and Venus Express that had minimum orbital altitudes of ~160 km and ~130 km, respectively, we observe equivalent $\Delta V s$ of a few mm s^{-1}. The difference $|\Delta V_{VGRAM} - \Delta V_{VCD}|$ for the EnVision mission reaches 0.16 mm s^{-1} with a uniform distribution in the range of 0.06 and 0.13 mm s^{-1}. This differential velocity is accumulated every orbit leading to significant effects on the orbit integration of the 4-days arc. The uniform distribution observed for the ΔV differences resulting from the two independent atmospheric models suggests that a single scale factor would not be well-suited to fully mitigate the effects associated with atmospheric mismodeling. This effect, however, can be absorbed or mitigated through an over-parameterization that could be the adjustment of multiple C_D per arc, or stochastic accelerations. This approach would inflate the uncertainties of the geophysical parameters estimation and the spacecraft's orbit (see Section 5).

4. Numerical simulations of the EnVision radio science investigation

4.1. Perturbative analysis

We performed a comprehensive set of numerical simulations of the entire mission science phase of six Venusian days. This dataset is analyzed by accounting for 300 arcs that are 4 days long. To investigate the impact of the current uncertainties in the knowledge of Venus' atmosphere on the determination of the spacecraft orbit and

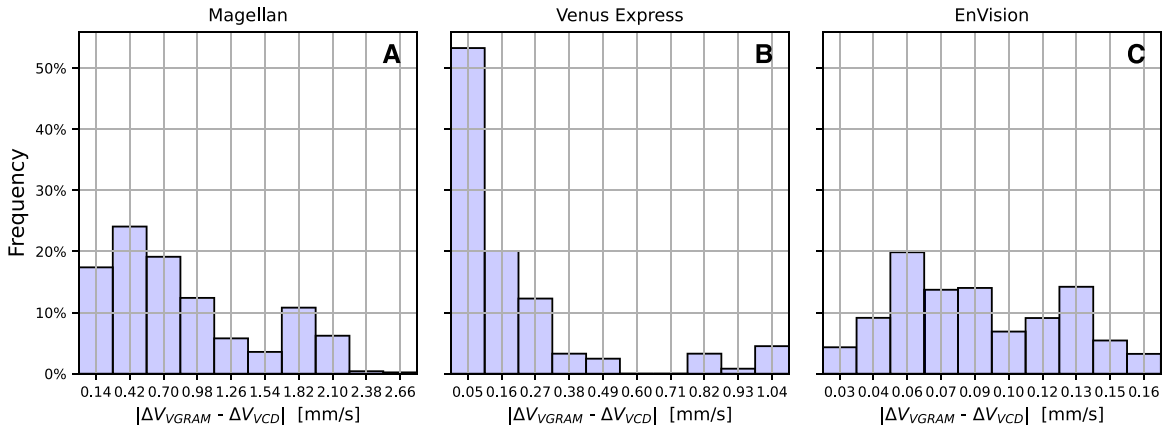

Fig. 4. Discrepancies between the equivalent ΔVs due to the atmospheric drag computed by using the Venus-GRAM and VCD for Magellan (Cycle 5) (left), Venus Express (center) and EnVision (right). Panels A, B and C report the frequency of the $|\Delta V_{VGRAM} - \Delta V_{VCD}|$ values that have been computed for each orbit during an entire Venusian cycle.

Venus' geophysical parameters, we carried out a perturbative analysis that accounts for the differences between the two atmospheric models Venus-GRAM and VCD. The POD software adopted in this study, the JPL MONTE Project Edition, includes the 2005 version of the Venus-GRAM. We also used the VCD to compute the atmospheric densities, and, consequently, the different prediction of the atmospheric drag acting on the spacecraft. These values can be provided to MONTE as tabular data by turning off the internal atmospheric model. This approach allows us to simulate possible discrepancies between predictions based on the semi-empirical model and the real value of the atmospheric properties. The discrepancies between the two atmospheric models are consistent with the level of uncertainties of those predictions, leading to a realistic test and validation of the proposed method.

A perturbative analysis consists in using different dynamical models between the numerical simulations for the generation of the synthetic data and for the POD analysis. This approach significantly differs from a covariance analysis that does not account for any perturbation in the dynamical model, leading to assess formal uncertainties only. Because of the short- and long-term variations of the atmospheric properties, a perturbative analysis is well-suited to better understand the effects of atmospheric mismodeling on the spacecraft trajectory reconstruction by studying the systematic errors. In our numerical simulations, we computed the synthetic Doppler measurements by using the tabular data with a 1-s sampling time for the atmospheric drag accelerations based on the VCD density predictions.

To compute the drag accelerations with the atmospheric densities ρ based on the VCD model, we provide as input the precise epoch, longitude and latitude coordinates, the distance to the planet center, the desired combination of cloud albedo and solar EUV scenarios and a flag to set additional perturbations, *e.g.* small scale (gravity waves) and large scale perturbations. The estimated ρ is then used to compute the drag acceleration accordingly to Eq. (5). Since the drag acceleration strongly perturbs the spacecraft trajectory leading to different values of atmospheric density, the use of tabular data to model the atmospheric drag accelerations requires an iterative approach. The convergence of the method is declared when the discrepancies between the trajectory adopted for the computation of the drag accelerations and the trajectory obtained applying the updated perturbations are negligible (*i.e.*, $\leq$ 1 mm).

For the analysis of the synthetic data to reconstruct the spacecraft orbit, we use the hard-coded atmospheric model Venus-GRAM 2005 available in MONTE to mimic the future POD process with real data. The other force models are identical between simulation and estimation process to only study the effects of atmospheric drag mismodeling.

4.2. Estimation strategies

The perturbations associated with non-conservative forces are compensated by using different approaches, including the estimation of additional local parameters. Previous radio science investigations on Venus and Mars [29,35,49] have estimated a set of local parameters (*e.g,* periodic accelerations, drag scale factors) through a single-arc batch least-squares solution. This approach, however, leads to a significant over-parameterization that may affect the adjustment of the global parameters, including the gravitational field and tides.

We then propose a method that enables the estimation of a limited number of local parameters by including the retrieval of atmospheric model scale factors (*e.g.*, [49]), which may provide unprecedented measurements of the Venus' atmosphere at the spacecraft altitude. The coefficients that have been considered in our analysis to cope with atmospheric drag mismodeling include spacecraft's drag coefficient C_D^{est}, which is modeled by using a constant term and a linear term ($C_D^{est} = C_{D_0}^{est} + \dot{C}_D^{est}\Delta t$); furthermore, we adjust scaling factors a_i that are associated with different altitude bands of Venus' atmosphere and multiply the nominal density provided by theoretical models $\rho^{est} = (C_D^{est}/C_D^*)a_i\rho_{VGRAM}$, ($C_D^*$ is the *a priori* value of the spacecraft's C_D). This technique is based on the batch-sequential filtering presented in Section 2.2.2.

To study the benefits of the proposed method, we carried out numerical simulations based on the combined processing of the arcs through a batch filter that includes the adjustment of periodic accelerations or drag scale factors (Section 4.2.1) and the batch-sequential filter that enables the estimation of atmospheric scale factors (Section 4.2.2).

Tables 1 and 2 show the local and global parameters estimated through the two techniques with the associated *a priori* uncertainties. Local parameters include the spacecraft's state vector (*i.e.*, position and velocity) and an impulsive ΔV per day uniformly distributed along the three spacecraft body axes to account for WoL maneuvers. The additional local parameters that are adjusted with the two methods are periodic accelerations, and the scale factor and linear term for the C_D. In the global iterations, we estimate the gravity field in spherical harmonics to degree and order 50, the real part of the Love number k_2 and the tidal phase lag Φ. For the batch-sequential filter, the global parameters also include atmospheric scale factors at different altitudes enabling the characterization of the atmospheric density profiles.

4.2.1. Batch filter with local over-parameterization

To compensate for errors in the modeling of the spacecraft's dynamics, periodic accelerations are first included in the set of estimated local parameters. These accelerations are modeled as the sum of sinusoidal and cosinusoidal terms acting in the Radial, Transverse and Normal directions (R-T-N) with period equal to the orbital period. The periodic

Table 1
Local and global parameters included in the least-squares filter.

	Least-squares batch filter	
	Single Arc estimate *a priori* 1σ	Global inversion *a priori* 1σ
Local parameters		
Spacecraft position	300 m	
Spacecraft velocity	10 cm/s	
Impulse burns	1 mm/s	
Periodic accelerations or spacecraft C_D	10^{-6} m/s^2 or unconstrained	
Global parameters		
Gravity field		
Love number k_2	N/A	Unconstrained
Tidal phase lag ϕ		

Table 2
Local and global parameters included in the batch-sequential filter.

	Batch-sequential filter		
	Single arc estimate *a priori* 1σ	Intermediate global inversion *a priori* 1σ	Final global inversion *a priori* 1σ
Local parameters			
Spacecraft position	300 m		
Spacecraft velocity	10 cm/s		
Impulse burns	1 mm/s		
Spacecraft C_D scale factor	Unconstrained		
Spacecraft C_D linear term	Unconstrained		
Global parameters			
Atmospheric scale factor 220–320 km			
Atmospheric scale factor 320–420 km	N/A	Unconstrained	Unconstrained
Atmospheric scale factor 420–520 km			
Gravity field			
Love number k_2	N/A	N/A	Unconstrained
Tidal phase lag ϕ			

accelerations are included in the POD process by re-initializing the coefficients of the sinusoidal and cosinusoidal terms with an update time of 1 day and *a priori* uncertainty $\sigma = 10^{-6}$ m/s^2, corresponding to a $2-\sigma$ of the maximum error observed between the VCD and Venus-GRAM models. This method leads to the estimation of 24 additional local parameters, adding then ~7200 parameters in the global inversion.

After a single-arc estimation, a global iteration enables the inversion of the global parameters. Our results show that the additional set of periodic accelerations is not sufficient to precisely reconstruct the spacecraft orbit (Figure S8). This approach would also prevent an accurate characterization of the atmospheric density variability.

To extend the scientific return of the radio science investigation, a consolidated strategy in POD solutions consists in the adjustment of parameters that directly affect the computation of the drag acceleration. We then estimate one drag scale factor C_D per each orbit that is ~1.5 h long. This approach then accounts for an additional set of 64 local parameters per arc with an unconstrained *a priori* uncertainties.

This extreme over-parameterization that includes ~19000 additional parameters in the global inversion enables an accurate estimation of the gravity field, as shown in Fig. 5. The estimation errors, which are computed as the absolute value of the differences between the estimated and *a priori* field, are within the $3-\sigma$ boundary. The drag scale factors (Figure S9) included in the estimation process allow us then to correct the dynamical errors that would affect the determination of the geophysical parameters. As expected, the filter yields C_D values that are lower than the nominal value ($C_D^* = 1.8$) to compensate the Venus-GRAM larger atmospheric density predictions at the spacecraft periapsis compared to the VCD. Fig. 6 shows that with this estimation strategy the RMS of the Doppler residuals is in agreement with the simulated measurement noise.

4.2.2. Batch-sequential filter with adjustment of the atmospheric model

The batch-sequential filter developed in this work is adopted to sequentially update a set of global parameters that characterize Venus' atmosphere. We adjust three scale factors associated with three altitude regions that are 220–320 km, 320–420 km and 420–520 km to cope with long-term variation of the atmospheric mismodeling. This method allows us to obtain a good fit of the simulated data by including a limited number (*i.e.*, 8 per arc) of additional local parameters that are one scale factor and linear rate of the drag coefficient (C_D) per day (Table 2).

Different tests have been carried out to determine the number of arcs to include in each batch. By starting with a number of arcs between 10 and 15, unstable solutions were retrieved in the global inversion because the radio tracking data were not enough to constrain the atmospheric properties. We note that the atmospheric scale factors can be preliminary estimated through the analysis of radio science data after one third of a Venus' cycle that corresponds to a batch length of ~ 20 arcs. This time span is well-suited to sample the range of altitudes crossed by the spacecraft. An intermediate global estimate of the atmospheric parameters is then carried out to refine and improve the dynamical models adopted for the following batches. However, a thorough characterization of the spatial and temporal variability of the upper atmosphere's density is only obtained through a sequential update of the adjusted parameters after 12 batches. At the end of the batch-sequential filter, we reprocess each single arc with the updated atmospheric model, and a final global estimate is carried out to retrieve the gravity field coefficients, Love number k_2 and its phase lag Φ. This approach leads to an accurate fit of the Doppler measurements as shown by their residuals that are fully consistent with the expected level of noise (orange dots in Fig. 6). The estimate of the gravity field parameters is accurately determined with estimated errors within three-standard-deviation ($3-\sigma$) uncertainty level (Fig. 5, orange). An improvement is also observed for the formal uncertainty of the gravity field thanks to the lower number of adjusted parameters compared to the batch filter with one adjusted C_D per orbit. A further improvement is also observed on the estimation of Venus' tidal response

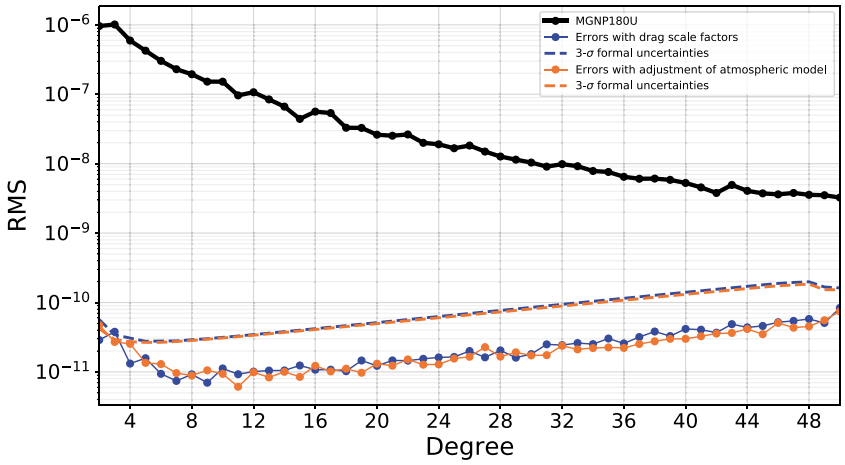

Fig. 5. Power spectrum of the Venus' gravity field MGNP180U used as *a priori* model in this study (**black**), of the formal uncertainties of the estimated gravity field (**dashed blue line**) and the errors (**dotted blue line**) obtained by estimating an atmospheric drag coefficient per orbit, and of the formal uncertainties and the errors obtained by adjusting the atmospheric model (orange). (For interpretation of the references to color in this figure legend, the reader is referred to the web version of this article.)

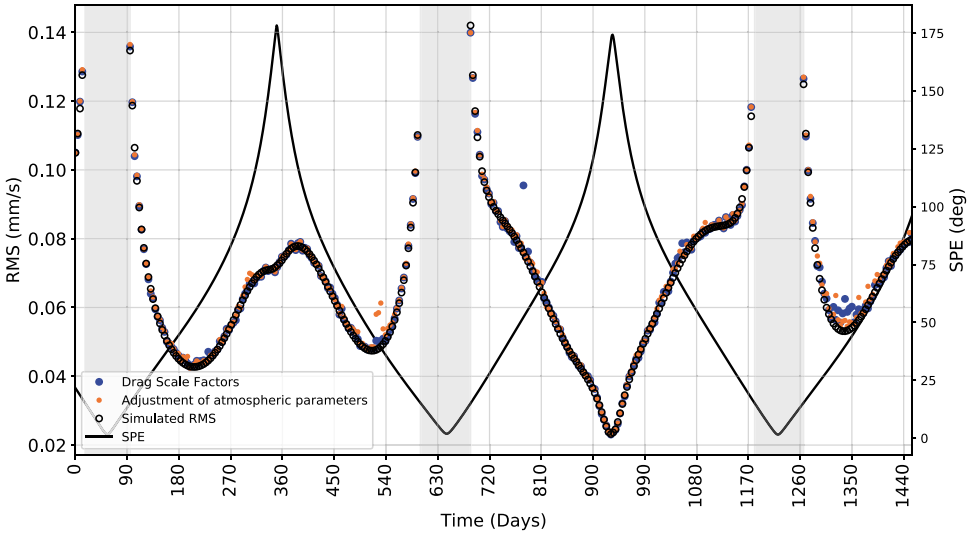

Fig. 6. Doppler measurement noise (**black circles**) and residuals for the simulated science phase of the EnVision mission. The numerical simulations are based on the adjustment of one C_D per orbit in a batch filter (**blue**) and of the atmospheric model through the batch-sequential filtering (**orange**). The gray shaded areas correspond to superior solar conjunctions that corresponds to $SPE \leq 15°$ (**black line**). (For interpretation of the references to color in this figure legend, the reader is referred to the web version of this article.)

(see Section 5). The approach presented in this study is tailored to process real data in the Venusian environment since mismodeling of the dynamical perturbations is accounted for and adjusted to enhance the estimation of both local and global parameters with respect to a standard technique based on single global inversion.

5. Discussion

The batch-sequential processing of the radio tracking data of the EnVision mission provides a solid strategy to deal with mismodeling in the spacecraft dynamics, including the atmospheric drag accelerations. Our results show that an adequate over-parameterization is also well-suited to fully mitigate the dynamical errors. However, the batch-sequential filter based on intermediate adjustments of the atmospheric model, which is the source of the dynamical errors, enables comparable results by accounting for a limited set of estimated local parameters. The reduced number of adjusted parameters leads to better constrain the gravity field and tides and to refined modeling of Venus' atmospheric density. The batch filter based on the adjustment of one C_D per orbit leads to a $3-\sigma$ uncertainty of $3.0 \cdot 10^{-3}$ and $2.6 \cdot 10^{-1}$ deg for the Love number k_2 and its phase lag Φ, respectively. An improvement of a factor of 2 and of ~30% is obtained with the batch-sequential estimator for the tidal amplitude ($1.5 \cdot 10^{-3}$) and phase ($1.9 \cdot 10^{-1}$ deg), respectively. These simulations enable a relative comparison between the different estimation strategies. We note that the reported uncertainties are based on the global inversion of Venus' gravity field to degree and order 50. Therefore, larger uncertainties are expected if the global estimation includes the gravitational harmonics to degree and order 180 consistently with our previous numerical simulations [20].

A major strength of the proposed method is the characterization of Venus' atmospheric density ρ through the analysis of the radio tracking data. To better understand the quality of our reconstructed atmospheric properties, we compare the atmospheric densities predicted by the VCD (ρ_{VCD} in Fig. 7A), which is our ground truth model for the generation of the synthetic measurements, with the reconstructed densities obtained through a batch least-squares filter with one C_D per orbit and the batch-sequential filter with the adjustment of atmospheric scale factors. In both estimation strategies, we estimate the drag scale coefficient that is assumed constant ($C_D^* = 1.8$) in the ground truth model. The compensation of atmospheric mismodeling is obtained through the combination

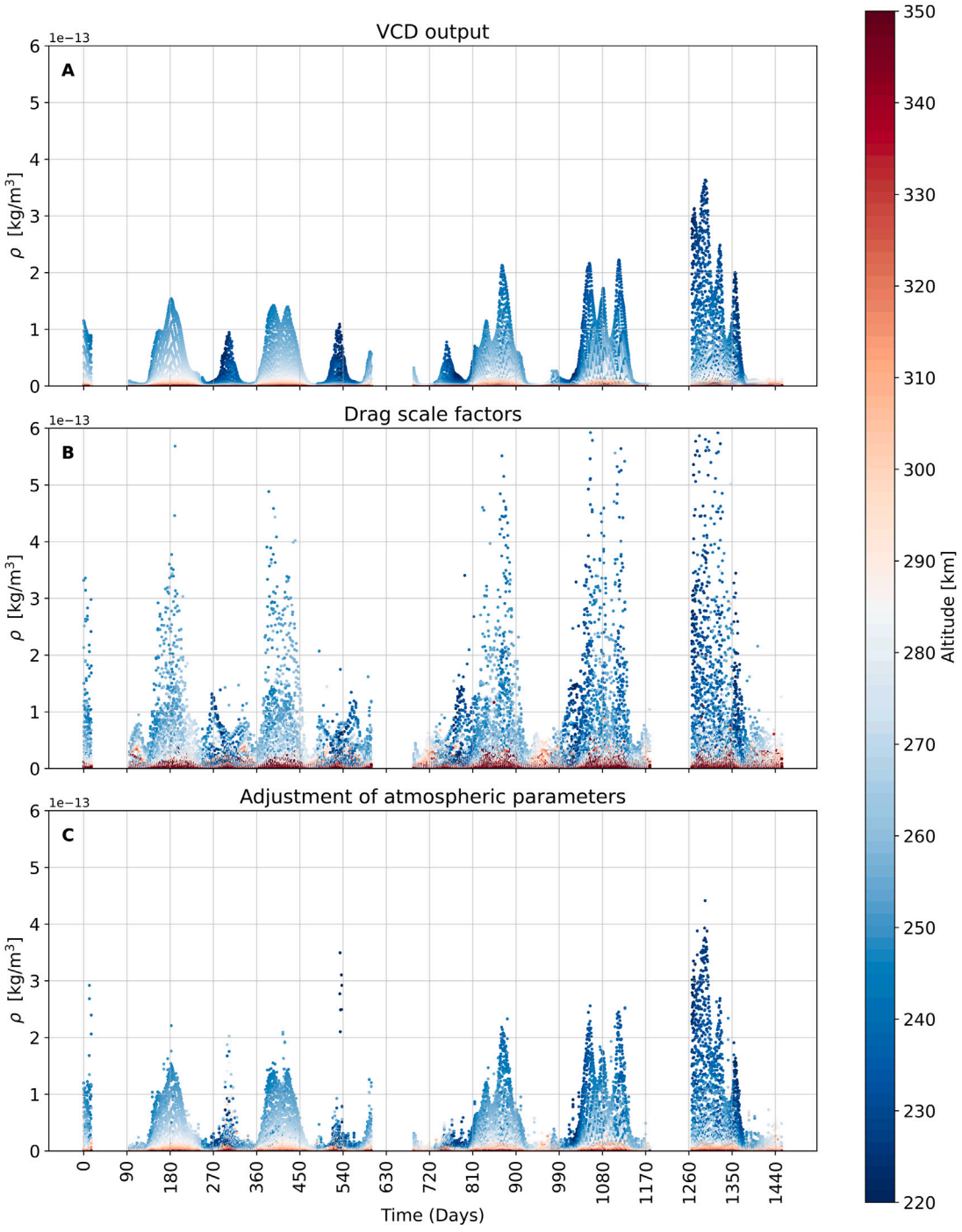

Fig. 7. Reconstructed evolution of the density ρ during the mission timespan (days after 15 June 2035). Panel A shows the simulated ρ, obtained by using the VCD. Panel B shows the values of ρ estimated by using the Venus GRAM and adjusting a C_D scale factor per orbit through the least-squares filter. Panel C reports the values of ρ estimated by using the Venus GRAM and updating a C_D scale factor and linear term per day and scale factors for three altitude regions of Venus' atmosphere through the batch-sequential filter.

of the drag scale factor C_D^{est} and, if included among the estimation parameters, its linear rate $\dot{C}_D^{est}$ and the atmospheric scale factors. The estimated density ρ^{est} for the two approaches (*i.e.*, least-squares, LS, and batch-sequential, BS) is thus given by

$$\rho_{LS}^{est}(t) = \frac{C_D^{est}(t)}{C_D^*}\ \rho_{VGRAM}, \quad \rho_{BS}^{est} = \frac{C_{D_0}^{est}(t) + \dot{C}_D^{est}(t)\Delta t}{C_D^*}\ a_i\ \rho_{VGRAM} \quad i = 1, 2, 3, \tag{7}$$

where ρ_{VGRAM} is the atmospheric density value predicted by the *a priori* model in the MONTE software (*i.e.*, Venus-GRAM 2005). The scale and linear rate of the drag scale factor are step functions with respect to time depending on the assumed discretization that is one per orbit for the LS and one per day for the BS. The parameter a_i is the atmospheric scale factor for each altitude range considered in this study by accounting for three 100-km ranges from the spacecraft periapsis altitude (*i.e.*, a_1 for 220–320 km, a_2 for 320–420 km, and a_3 for 420–520 km). Fig. 7B shows the estimated density profile through

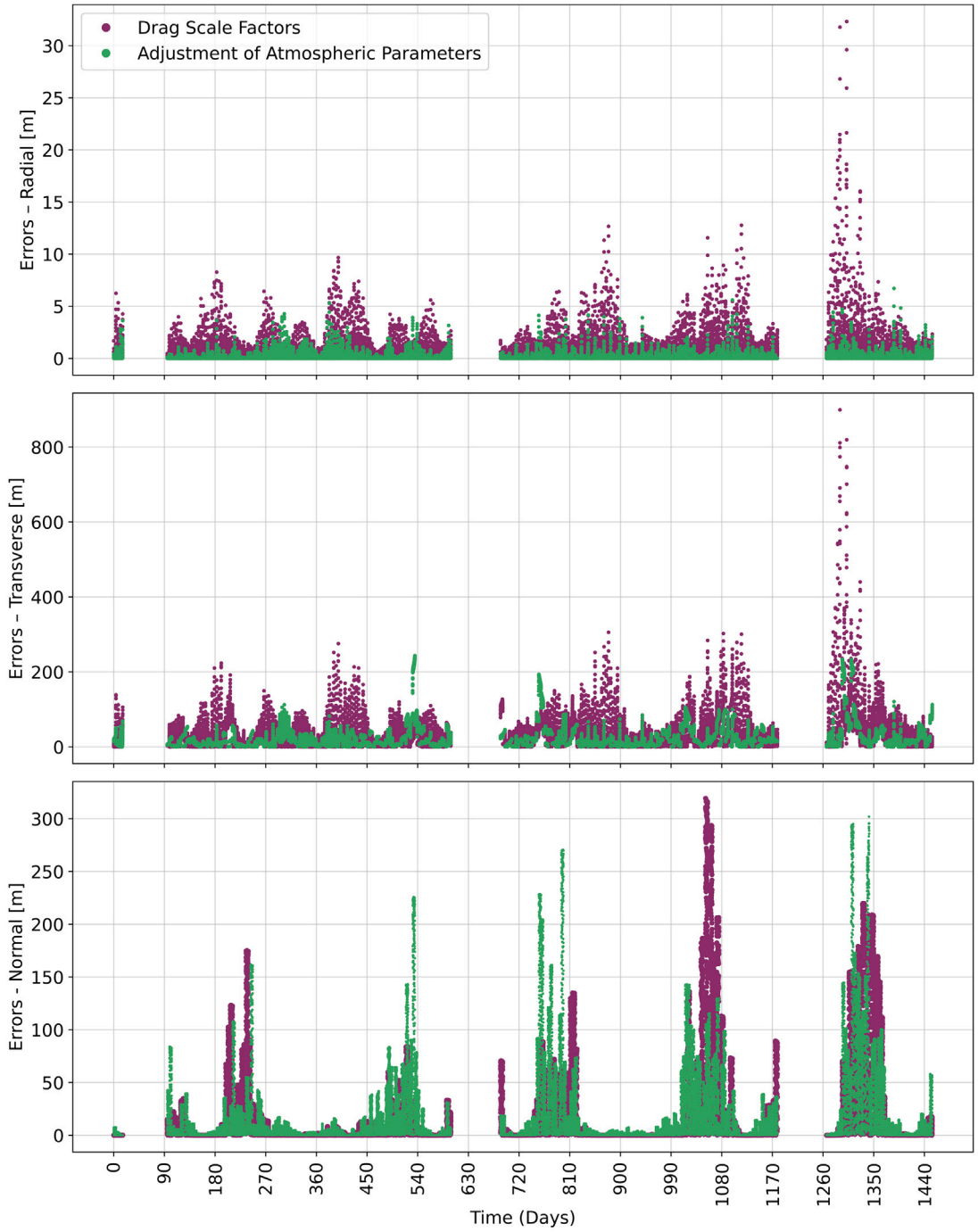

Fig. 8. Absolute values of the errors on the reconstructed trajectory projected in the Radial, Transverse and Normal directions (R-T-N) computed by adjusting a C_D scale factor per orbit through the LS filter (**purple**) and by updating the atmospheric parameters through the BS filter (**green**). (For interpretation of the references to color in this figure legend, the reader is referred to the web version of this article.)

the significant over-parameterization of the drag scale factors per each arc. A significant scattering of the measurements is observed for the entire mission time span, leading to atmospheric measurements that are covered by a strong noise. This estimation strategy is then well-suited to compensate those mismodeling for the gravity field inversion but it prevents us from gathering any information on the atmospheric properties.

The atmospheric densities estimated by using the batch-sequential filter with the retrieval of the atmospheric scale factors provide accurate results that are fully consistent with the ground truth model (Fig. 7C). The global parameters included in the inversion of the 20-arcs batches enable the compensation of long-term variabilities that are poorly predicted by the prior modeling of the atmosphere. The estimation of the local parameters C_D^{est} and $\dot{C}_D^{est}$ in the single-arc

analysis is important to mitigate short-term temporal variations of the atmospheric density. A full calibration of the atmospheric mismodeling is then obtained after the final inversion that accounts for the adjusted local and global scale factors. The proposed approach yields an accurate determination of the atmospheric density with formal uncertainties of ∼ 25%. We note that the *a priori* errors on the atmospheric densities, which result from the differences between VCD and Venus-GRAM, are on average > 200%.

Our results thus suggest that the retrieved ρ_{BS}^{est} can be used to enhance the semi-empirical model providing unprecedented measurements of Venus' atmosphere at the spacecraft orbit altitudes. Venus' thermosphere region usually lacks *in situ* observations provided by spectrometers and data derived from radio occultation experiments or from the orbital decay of the probe. Thanks to EnVision orbital configuration and the enhanced spectrometers suite (VenSpec) with respect to Venus Express, an higher resolution and spatially uniform characterization of Venus' atmosphere in the altitude range 0–50 km is expected. The lower atmosphere and cloud top layer (35–100 km) will be investigated through the EnVision radio-occultation experiment. The observed shift in the frequency of the Doppler signal received on Earth, which results from the bending of the radio link due to the neutral atmosphere, will infer the atmospheric density, temperature, pressure absorption and composition in that altitude band. Thus, the information retrieved through the Doppler tracking data analysis would be complementary to the data measured by dedicated instrumentation and extremely valuable for investigations of Venus' atmosphere.

A better knowledge of the dynamical model leads to a more accurate reconstruction of the spacecraft trajectory. By comparing the simulated trajectory based on the ground truth model with the trajectory retrieved with LS and BS, we observe significant improvements of the spacecraft position estimation with the adjustment of the atmospheric parameters. Fig. 8 shows that the LS with the estimation of one drag scale factor per orbit leads to average errors of 4–5 m, 100 m and 30 m in the radial, transverse and normal direction, respectively. During the final mission science phase analyzed in this study, when the atmospheric density significantly increases, the orbital errors are dramatically inflated. The BS with the refinement of the atmospheric properties leads to a precise estimation of the spacecraft position with radial, transverse and normal errors of 1–2 m, 30–40 m and 20–30 m on average, respectively. No differences are observed at the end of the mission phase. Our results support that the proposed technique allows us to fulfill the spacecraft trajectory requirements, which are also pivotal for the other EnVision instruments.

6. Summary

Understanding how Venus has evolved and whether it is still active today are the main objectives of the EnVision mission. To fulfill the scientific requirements, the EnVision spacecraft will be inserted in a low-altitude orbit and will investigate the geological and atmospheric processes supporting the determination of Venus' geophysical parameters through the radio science investigation. The analysis of the radiometric data is strongly dependent on our knowledge of the spacecraft's dynamical modeling. A precise modeling of the conservative (*e.g.*, gravitational force) and non-conservative forces (*e.g.*, atmospheric drag, attitude control maneuvers, solar radiation pressure, albedo and thermal emissivity) is fundamental to accurately reconstruct the spacecraft's trajectory and consequently to estimate Venus's geophysical parameters.

In this work, we investigated the impact of the current uncertainties in the knowledge of Venus' atmosphere on the EnVision gravity investigation. By introducing a mismodeling of the drag acceleration consistent with the uncertainties in the prediction of the atmospheric properties, we assessed the effects of expected dynamical errors on the estimation of the spacecraft's orbital evolution. The results of our numerical simulations suggest that the effect of such mismodeling is not negligible at the spacecraft periapsis altitude. The adoption of a classical least-squares filter would require the estimation of a large number of local parameters (64 additional parameters per arc, *i.e.*, a drag coefficient per orbit) to compensate for the atmospheric mismodeling.

An alternative approach proposed in this work for the POD allows the joint determination of Venus' geophysical parameters and atmospheric density profiles. This method consists in processing smaller batches of data and to sequentially improve the dynamical model through the estimation of global parameters that compensate the atmospheric density mismodeling. A set of additional local parameters is also adjusted in each arc to mitigate local variabilities of the atmospheric properties. The batch-sequential filter allows us to accurately estimate the gravity field parameters that are consistent with the $3-\sigma$ uncertainties. By accurately adjusting the atmospheric density in three altitude ranges (*i.e.*, between 220–320 km, 320–420 km and 420–520 km) and the local C_D daily scale and linear factors, this method enables the reconstruction of Venus' density profiles at the spacecraft's orbital altitudes, yielding significant improvements on the POD solution. The information on the density variations in the thermosphere extends the scientific return of the radio science investigation of the EnVision mission. A better characterization of Venus' thermosphere is a key objective of the ESA mission to enhance our knowledge of the upper atmosphere.

Declaration of competing interest

The authors declare that they have no known competing financial interests or personal relationships that could have appeared to influence the work reported in this paper.

Acknowledgments

AG acknowledges the California Institute of Technology (Caltech) and the Jet Propulsion Laboratory (JPL) for the license of the software MONTE Project Edition [36], which has been used by AMG, FP, AG, EDV, SA and TT to carry out the numerical simulations of the ESA mission EnVision. AG, AMG, FP, EDV, SA and TT acknowledge funding from the Italian Space Agency (ASI) grant n. 2023-60-HH.0.

Appendix A. Supplementary data

Supplementary material related to this article can be found online at https://doi.org/10.1016/j.actaastro.2023.12.010.

References

[1] J.B. Garvin, S.A. Getty, G.N. Arney, N.M. Johnson, E. Kohler, K.O. Schwer, M. Sekerak, A. Bartels, R.S. Saylor, V.E. Elliott, C.S. Goodloe, M.B. Garrison, V. Cottini, N. Izenberg, R. Lorenz, C.A. Malespin, M. Ravine, C.R. Webster, D.H. Atkinson, S. Aslam, S. Atreya, B.J. Bos, W.B. Brinckerhoff, B. Campbell, D. Crisp, J.R. Filiberto, F. Forget, M. Gilmore, N. Gorius, D. Grinspoon, A.E. Hofmann, S.R. Kane, W. Kiefer, S. Lebonnois, P.R. Mahaffy, A. Pavlov, M. Trainer, K.J. Zahnle, M. Zolotov, Revealing the mysteries of Venus: The DAVINCI mission, Planet. Sci. J. 3 (5) (2022) 117, http://dx.doi.org/10.3847/psj/ac63c2.

[2] S.E. Smrekar, S. Hensley, M.D. Dyar, J. Whitten, D. Nunes, J. Helbert, L. Iess, E. Mazarico, J. Andrews-Hanna, D. Breuer, D. Buczkowski, B. Campbell, A. Davaille, G. Di Achille, C.I. Fassett, M. Gilmore, R. Herrick, L. Jozwiak, T. Kataria, A. Konopliv, M. Mastrogiuseppe, N. Mueller, M. Raguso, J. Stock, E. Stofan, T. Widemann, H. Zebker, VERITAS (Venus Emissivity, Radio Science, InSAR, Topography, and Spectroscopy: Surface science objectives, in: LPI Contributions, vol. 2807, 2023, p. 8014.

[3] R. Ghail, C. Wilson, T. Widemann, L. Bruzzone, C. Dumoulin, J. Helbert, R. Herrick, E. Marcq, P. Mason, P. Rosenblatt, A. Vandaele, L.-J. Burtz, EnVision: Understanding why our most Earth-like neighbour is so different, 2017, arXiv:1703.09010.

[4] ESA, EnVision Understanding Why Earth's Closest Neighbour Is So Different. Assessment Study Report (Yellow Book), 2021, pp. 1–111, ESA/SCI(2021)1.

[5] H. Lammer, A. Zerkle, S. Gebauer, N. Tosi, L. Noack, M. Scherf, E. Pilat-Lohinger, M. Güdel, J.L. Grenfell, M. Godolt, A. Nikolaou, Origin and evolution of the atmospheres of early Venus, Earth and Mars, Astron. Astrophys. Rev. 26 (1) (2018) 2, http://dx.doi.org/10.1007/s00159-018-0108-y.

[6] H. Masursky, E. Eliason, P.G. Ford, G.E. McGill, G.H. Pettengill, G.G. Schaber, G. Schubert, Pioneer Venus radar results: Geology from images and altimetry, J. Geophys. Res. Space Phys. 85 (A13) (1980) 8232–8260, http://dx.doi.org/10.1029/JA085iA13p08232.

[7] R.G. Prinn, The volcanoes and clouds of Venus, Sci. Am. 252 (3) (1985) 46–53, URL http://www.jstor.org/stable/24967591.

[8] R.G. Strom, G.G. Schaber, D.D. Dawson, The global resurfacing of Venus, J. Geophys. Res.: Planets 99 (E5) (1994) 10899–10926, http://dx.doi.org/10.1029/94JE00388.

[9] P.K. Byrne, R.C. Ghail, M.S. Gilmore, A.C. Şengör, C. Klimczak, D.A. Senske, J.L. Whitten, S. Khawja, R.E. Ernst, S.C. Solomon, Venus tesserae feature layered, folded, and eroded rocks, Geology 49 (1) (2020) 81–85, http://dx.doi.org/10.1130/G47940.1.

[10] R.R. Herrick, S. Hensley, Surface changes observed on a Venusian volcano during the Magellan mission, Science 379 (6638) (2023) 1205–1208, http://dx.doi.org/10.1126/science.abm7735.

[11] S.E. Smrekar, E.R. Stofan, N. Mueller, A. Treiman, L. Elkins-Tanton, J. Helbert, G. Piccioni, P. Drossart, Recent hotspot volcanism on Venus from VIRTIS emissivity data, Science 328 (5978) (2010) 605–608, http://dx.doi.org/10.1126/science.1186785.

[12] E. Marcq, J.-L. Bertaux, F. Montmessin, D. Belyaev, Variations of sulphur dioxide at the cloud top of Venus's dynamic atmosphere, Nat. Geosci. 6 (1) (2013) 25–28, http://dx.doi.org/10.1038/ngeo1650.

[13] J. Filiberto, D. Trang, A.H. Treiman, M.S. Gilmore, Present-day volcanism on Venus as evidenced from weathering rates of olivine, Sci. Adv. 6 (1) (2020) eaax7445, http://dx.doi.org/10.1126/sciadv.aax7445.

[14] A.S. Konopliv, W.B. Banerdt, W.L. Sjogren, Venus gravity: 180th degree and order model, Icarus 139 (1999) 3–18, http://dx.doi.org/10.1006/icar.1999.6086.

[15] A.S. Konopliv, C.F. Yoder, Venusian k2 tidal Love number from Magellan and PVO tracking data, Geophys. Res. Lett. 23 (1996) 1857–1860, http://dx.doi.org/10.1029/96GL01589.

[16] C. Dumoulin, G. Tobie, O. Verhoeven, P. Rosenblatt, N. Rambaux, Tidal constraints on the interior of Venus, J. Geophys. Res.: Planets 122 (6) (2017) 1338–1352, http://dx.doi.org/10.1002/2016JE005249.

[17] J.-L. Margot, D.B. Campbell, J.D. Giorgini, J.S. Jao, L.G. Snedeker, F.D. Ghigo, A. Bonsall, Spin state and moment of inertia of Venus, Nat. Astron. 5 (7) (2021) 676–683, http://dx.doi.org/10.1038/s41550-021-01339-7.

[18] C. Xiao, F. Li, J. Yan, M. Gregoire, W. Hao, Y. Harada, M. Ye, J.-P. Barriot, Possible deep structure and composition of Venus with respect to the current knowledge from geodetic data, J. Geophys. Res.: Planets 126 (7) (2021) http://dx.doi.org/10.1029/2019JE006243, e2019JE006243.

[19] F. Petricca, A. Genova, S. Goossens, L. Iess, G. Spada, Constraining the internal structures of Venus and Mars from the gravity response to atmospheric loading, Planet. Sci. J. 3 (7) (2022) 164–187, http://dx.doi.org/10.3847/PSJ/ac7878.

[20] P. Rosenblatt, C. Dumoulin, J.-C. Marty, A. Genova, Determination of Venus' interior structure with EnVision, Remote Sens. 13 (9) (2021) 1624, http://dx.doi.org/10.3390/rs13091624.

[21] A.J. Kliore, V.I. Moroz, G.M. Keating, The Venus International Reference Atmosphere, 5, Pergamon Press, Elmsford, 1985, pp. 1–305,

[22] S. Lebonnois, F. Hourdin, V. Eymet, A. Crespin, R. Fournier, F. Forget, Superrotation of Venus' atmosphere analyzed with a full general circulation model, J. Geophys. Res. (Planets) 115 (E6) (2010) E06006, http://dx.doi.org/10.1029/2009JE003458.

[23] S.S. Limaye, S. Lebonnois, A. Mahieux, M. Pätzold, S. Bougher, S. Bruinsma, S. Chamberlain, R.T. Clancy, J.-C. Gérard, G. Gilli, D. Grassi, R. Haus, M. Herrmann, T. Imamura, E. Kohler, P. Krause, A. Migliorini, F. Montmessin, C. Pere, M. Persson, A. Piccialli, M. Rengel, A. Rodin, B. Sandor, M. Sornig, H. Svedhem, S. Tellmann, P. Tanga, A.C. Vandaele, T. Widemann, C.F. Wilson, I. Müller-Wodarg, L. Zasova, The thermal structure of the Venus atmosphere: Intercomparison of Venus Express and ground based observations of vertical temperature and density profiles, Icarus 294 (2017) 124–155, http://dx.doi.org/10.1016/j.icarus.2017.04.020.

[24] L.V. Zasova, V.I. Moroz, V. Formisano, N.I. Ignatiev, I.V. Khatuntsev, Exploration of Venus with the Venera-15 IR Fourier spectrometer and the Venus Express planetary Fourier spectrometer, Cosmic Res. 44 (4) (2006) 349–363, http://dx.doi.org/10.1134/S0010952506040083.

[25] J.-L. Bertaux, D. Nevejans, O. Korablev, E. Villard, E. Quémerais, E. Neefs, F. Montmessin, F. Leblanc, J. Dubois, E. Dimarellis, A. Hauchecorne, F. Lefèvre, P. Rannou, J. Chaufray, M. Cabane, G. Cernogora, G. Souchon, F. Semelin, A. Reberac, E. Van Ransbeek, S. Berkenbosch, R. Clairquin, C. Muller, F. Forget, F. Hourdin, O. Talagrand, A. Rodin, A. Fedorova, A. Stepanov, I. Vinogradov, A. Kiselev, Y. Kalinnikov, G. Durry, B. Sandel, A. Stern, J. Gérard, SPICAV on Venus Express: Three spectrometers to study the global structure and composition of the Venus atmosphere, Planet. Space Sci. 55 (12) (2007) 1673–1700, http://dx.doi.org/10.1016/j.pss.2007.01.016.

[26] S. Tellmann, M. Pätzold, B. Häusler, M.K. Bird, G.L. Tyler, Structure of the Venus neutral atmosphere as observed by the radio science experiment VeRa on Venus Express, J. Geophys. Res.: Planets 114 (E9) (2009) http://dx.doi.org/10.1029/2008JE003204.

[27] G.M. Keating, R.H. Tolson, E.W. Hinson, Venus thermosphere and exosphere: First satellite drag measurements of an extraterrestrial atmosphere, Science 203 (4382) (1979) 772–774, http://dx.doi.org/10.1126/science.203.4382.772.

[28] N.C. Hsu, G.M. Keating, W.W. H., First Magellan measurements of the Venus thermosphere, EOS, Trans. AGU 73 (1992) 332.

[29] P. Rosenblatt, S.L. Bruinsma, I.C.F. Müller-Wodarg, B. Häusler, H. Svedhem, J.C. Marty, First ever in situ observations of Venus' polar upper atmosphere density using the tracking data of the Venus Express Atmospheric Drag Experiment (VExADE), Icarus 217 (2) (2012) 831–838, http://dx.doi.org/10.1016/j.icarus.2011.06.019, Advances in Venus Science.

[30] A. Genova, M. Marabucci, L. Iess, A batch-sequential filter for the BepiColombo radio science experiment, J. Aerosp. Eng. Sci. Appl. ISSN 2236-577X 4 (2012) 17–30, http://dx.doi.org/10.7446/jaesa.0404.02.

[31] ESA SPICE Service, EnVision SPICE Kernel Dataset, https://s2e2.cosmos.esa.int/bitbucket/projects/SPICE_KERNELS/repos/envision/.

[32] L. Iess, M. Di Benedetto, N. James, M. Mercolino, L. Simone, P. Tortora, Astra: Interdisciplinary study on enhancement of the end-to-end accuracy for spacecraft tracking techniques, Acta Astronaut. 94 (2) (2014) 699–707, http://dx.doi.org/10.1016/j.actaastro.2013.06.011.

[33] B. Bertotti, G. Comoretto, L. Iess, Doppler tracking of spacecraft with multi-frequency links, Astron. Astrophys. 269 (1993) 608–616.

[34] B.D. Tapley, B.E. Schutz, G.H. Born, Statistical Orbit Determination, Academic Press, Burlington, 2004, http://dx.doi.org/10.1016/B978-0-12-683630-1.X5019-X.

[35] A. Genova, S. Goossens, F.G. Lemoine, E. Mazarico, G.A. Neumann, D.E. Smith, M.T. Zuber, Seasonal and static gravity field of Mars from MGS, Mars Odyssey and MRO radio science, Icarus 272 (2016) 228–245, http://dx.doi.org/10.1016/j.icarus.2016.02.050.

[36] S. Evans, W. Taber, T. Drain, J. Smith, H.-C. Wu, M. Guevara, R. Sunseri, J. Evans, MONTE: The next generation of mission design and navigation software, CEAS Space J. 10 (2018) 79–86, http://dx.doi.org/10.1007/s12567-017-0171-7.

[37] W.M. Kaula, Theory of Satellite Geodesy: Applications of Satellites to Geodesy, in: Dover Earth Science Series, Dover Publications, 2000.

[38] M.A. Wieczorek, M. Meschede, SHTools: Tools for working with spherical harmonics, Geochem. Geophys. Geosyst. 19 (8) (2018) 2574–2592, http://dx.doi.org/10.1029/2018GC007529.

[39] B.A. Archinal, C.H. Acton, M.F. A'Hearn, A. Conrad, G.J. Consolmagno, T. Duxbury, D. Hestroffer, J.L. Hilton, R.L. Kirk, S.A. Klioner, D. McCarthy, K. Meech, J. Oberst, J. Ping, P.K. Seidelmann, D.J. Tholen, P.C. Thomas, I.P. Williams, Report of the IAU working group on cartographic coordinates and rotational elements: 2015, Celestial Mech. Dynam. Astronom. 130 (3) (2018) 22, http://dx.doi.org/10.1007/s10569-017-9805-5.

[40] W.M. Folkner, Planetary ephemeris DE432, 2014, Jet Propulsion Laboratory California Institute of Technology, Memorandum IOM 392R-14-003 (2014).

[41] J. Schofield, F. Taylor, Net global thermal emission from the Venusian atmosphere, Icarus 52 (2) (1982) 245–262, http://dx.doi.org/10.1016/0019-1035(82)90111-7.

[42] V.S. Meadows, D. Crisp, Ground-based near-infrared observations of the Venus nightside: The thermal structure and water abundance near the surface, J. Geophys. Res.: Planets 101 (E2) (1996) 4595–4622, http://dx.doi.org/10.1029/95JE03567.

[43] E. Gaposchkin, A. Coster, Evaluation of recent atmospheric density models, Adv. Space Res. 6 (9) (1986) 157–165, http://dx.doi.org/10.1016/0273-1177(86)90368-6.

[44] I.C.F. Müller-Wodarg, S. Bruinsma, J.-C. Marty, H. Svedhem, In situ observations of waves in Venus's polar lower thermosphere with Venus Express aerobraking, Nat. Phys. 12 (8) (2016) 767–771, http://dx.doi.org/10.1038/nphys3733.

[45] H. Justh, C. Justus, V. Keller, Global reference atmospheric models, including thermospheres, for Mars, Venus and Earth, in: AIAA/AAS Astrodynamics Specialist Conference and Exhibits, 2006, p. 6394.

[46] S. Lebonnois, N. Sugimoto, G. Gilli, Wave analysis in the atmosphere of Venus below 100-km altitude, simulated by the LMD Venus GCM, Icarus 278 (2016) 38–51, http://dx.doi.org/10.1016/j.icarus.2016.06.004.

[47] R. Haus, D. Kappel, G. Arnold, Atmospheric thermal structure and cloud features in the southern hemisphere of Venus as retrieved from VIRTIS/VEX radiation measurements, Icarus 232 (2014) 232–248, http://dx.doi.org/10.1016/j.icarus.2014.01.020.

[48] Y.J. Lee, K.L. Jessup, S. Pérez-Hoyos, D. Titov, S. Lebonnois, J. Peralta, T. Horinouchi, T. Imamura, S. Limaye, E. Marcq, M. Takagi, A. Yamazaki, M. Yamada, S. Watanabe, S.-y. Murakami, K. Ogohara, W. McClintock, G. Holsclaw, A. Roman, Long-term variations of Venus's 365 nm Albedo observed by Venus Express, Akatsuki, MESSENGER, and the Hubble Space Telescope, Astron. J. 158 (2019) 126, http://dx.doi.org/10.3847/1538-3881/ab3120.

[49] A. Genova, S. Goossens, F.G. Lemoine, E. Mazarico, S.K. Fricke, D.E. Smith, M.T. Zuber, Long-term variability of CO2 and O in the Mars upper atmosphere from MRO radio science data, J. Geophys. Res.: Planets 120 (5) (2015) 849–868, http://dx.doi.org/10.1002/2014JE004770.